Supporting Information

An inorganic capping strategy for the seeded growth of versatile bimetallic nanostructures

*Yuchen Pei, Raghu V. Maligal–Ganesh, Chaoxian Xiao, Tian–Wei Goh, Kyle Brahsler, Jeffrey A. Gustafson and Wenyu Huang**

[a] *Ames Laboratory, U.S. Department of Energy*
Department of Chemistry, Iowa State University, Ames, 50011, USA
E-mail: whuang@iastate.edu

1. Synthesis of $Pt@mSiO_2$

$Pt@mSiO_2$ was synthesized by following literature with some modifications.[1] 103 mg K_2PtCl_4 (Acros Organics) and 8.4 g tetradecyltrimethyl–ammonium bromide (TTAB, Sigma Aldrich) were dissolved in 200 mL H_2O with sonication. The cloudy solution was then placed in a 50 ˚C oil bath under vigorous stirring until a clear and homogenous Pt–TTAB solution appeared. 284 mg $NaBH_4$ (Alfa Aesar) was dissolved in 15 mL ice cold H_2O in advance. Aqueous $NaBH_4$ solution was then injected quickly into the clear Pt–TTAB mixture. After sealed with a septum, a needle was inserted to release the gas pressure. The mixture was kept under 50 ˚C with vigorous stirring for 24 hrs. The needle was removed after reacting 20 min. The brown Pt colloidal solution was centrifuged at 4000 rpm for 4 times (30 min each) to remove large Pt NPs. The uniform Pt nanoparticles (NPs) were then concentrated in around 20 mL H_2O after collecting the solids by centrifuging at 14000 rpm for 15 min twice. The concentrated Pt NPs aqueous solution was diluted to 150 mL with H_2O and 8 mL 0.05 M NaOH (EMD)/H_2O solution was added to obtain a pH of ~ 11. After stirring for 10 min, 3 mL 10% tetraethyl orthosilicate (TEOS, Sigma Aldrich) methanol solution was slowly added to the above Pt NPs–NaOH solution by using a syringe. The $Pt@mSiO_2$ was achieved after sealed and stirred for 24 hrs at room temperature. As–synthesized $Pt@mSiO_2$ was concentrated into 20 mL H_2O by centrifuge at 14000 rpm for 20 min twice. Further purification to remove surfactants was conducted in 150 mL 10 % HCl–methanol reflux at 90 ˚C for 24 hrs. After separation (14000 rpm, 20 min) and washing with methanol 3 times, $Pt@mSiO_2$ was obtained and stored in methanol.

2. Synthesis of $Pd@mSiO_2$

$Pd@mSiO_2$ was synthesized by following similar synthetic steps as $Pt@mSiO_2$. Pd NPs were obtained by the seeded growth approach. The Pd seed solution was made by mixing 250 µL 10 mM K_2PdCl_4/H_2O solution (Acros Organics), 450 µL 20 mM $NaBH_4$, 30 mg TTAB, and 9.3 mL H_2O. We then added 3 mL Pd seed solution and 20 mL 40 mM ascorbic acid (Sigma Aldrich) to a pre–made mixture of 25 mL 10 mM K_2PdCl_4 solution, 8.4 g TTAB, 38 mg NaI, and 200 mL H_2O in a 60 ˚C oil bath. The growth solution was kept at 60 ˚C with vigorous stirring for 3 hrs. Pd NPs were centrifuged at 3000 rpm for 3 times to remove large particles. Coating $mSiO_2$ shell process and methanol/HCl purification were conducted the same procedures as that for $Pt@mSiO_2$.

3. Seeded growth of bimetallic@$mSiO_2$ (PtM@$mSiO_2$)

Proper amounts of secondary metal precursors, such as $CuCl_2$ (J. T. Backer Chemicals), $Ni(NO_3)_2•6H_2O$ (Sigma Aldrich), $RhCl_3•xH_2O$ (Alfa Aesar) and K_2PdCl_4, were dissolved in 80 mL tetraethylene glycol (TEG, Fisher Scientific) to form a clear metal precursor–TEG solution. Proper volumes of $Pt@mSiO_2$ methanol solution were measured according to Pt metal quantity determined by ICP–MS. After centrifuging at 14000 rpm 20 min, the concentrated $Pt@mSiO_2$ was transferred into the above 80 mL metal–TEG solution (with small amounts of acetone added to help transfer). After sonication for dispersion, the brown TEG solution containing $Pt@mSiO_2$ and secondary metal precursor was then placed under vacuum to get rid of methanol and acetone remnants. After purging and protecting the solution with argon, the brown mixture was placed in a heating mantle with specific heating programs to reduce the secondary metal precursor on $Pt@mSiO_2$. After cooling down to room temperature, the $PtM@mSiO_2$–TEG solution was diluted twice its volume with acetone or methanol to help effective separation during centrifugation. $PtM@mSiO_2$ was collected by centrifuge and further washed with acetone or methanol 3 more times and stored in methanol for further characterization.

$PdPt@mSiO_2$ starting from $Pd@mSiO_2$ was synthesized via similar route using $Pd@mSiO_2$ as seeds instead and K_2PtCl_4 as the secondary metal precursor. The $PdPt@mSiO_2$ control synthesized in oleylamine by mixing $Pd@mSiO_2$ and H_2PtCl_6 (control v in Table 1) followed the similar synthetic conditions as that of the PtPd NPs control in Part 4.

The heating program for H_2PtCl_6, K_2PtCl_4, K_2PdCl_4 and $RhCl_3•xH_2O$: 30 ˚C to 180 ˚C in 1 hr, maintained at 180 ˚C for 2 hrs, and then ramping up to 280 ˚C in 2 hrs and maintained at 280 ˚C for another 2 hrs. For $Ni(NO_3)_2•6H_2O$ and $CuCl_2$, reaction solution was heated up to 280 ˚C in 2 hrs from 30 ˚C and maintained at 280 ˚C for another 2 hrs.

4. Seeded growth of PtPd NPs control

The major synthesis of PtPd NPs controls was followed by literature with modifications.[2] Pt or Pd NPs were synthesised as above and metal concentration was measured by ICP–MS. Normally, appropriate amounts of Pt or Pd NPs solutions (3 mg metal) was centrifuged and dispersed in 15 mL oleylamine (Sigma Aldrich), followed by the addition of $Pd(acac)_2$ (Sigma Aldrich) or H_2PtCl_6 (Acros Organics) with certain calculated ratios. The solution was heated up to 180 ˚C for 1 hr and maintained at 180 ˚C for 1 hr under argon protection. The dark brown mixture was separated and stored in ethanol or hexanes for further use. $PtPd/SiO_2$ catalyst was made by wetness impregnation. PtPd NPs ethanol/hexanes solution was loaded on silica gel (Sigma Aldrich) and dried (0.5 mg Pt/60 mg silica gel) in vacuum.

5. Si contents in the supernatant solution after synthesis

The Si contents of the supernatant solution were measured by ICP–MS using collision–induced dissociation mode under He flow to weaken the interference of COH species. After the synthesis, $Pt@mSiO_2$ and $PtPd@mSiO_2$ NPs were removed from the reaction solution via centrifugation, and the supernatant was then collected for ICP–MS. Typically, 5 mL of the supernatant was mixed with 5 µL of 50 wt.% HF at room temperature for overnight to dissolve $mSiO_2$. The HF–treated supernatant was then diluted with aqua regia and ultrapure water into certain concentration which is proper for ICP–MS analysis.

6. Figures and tables.

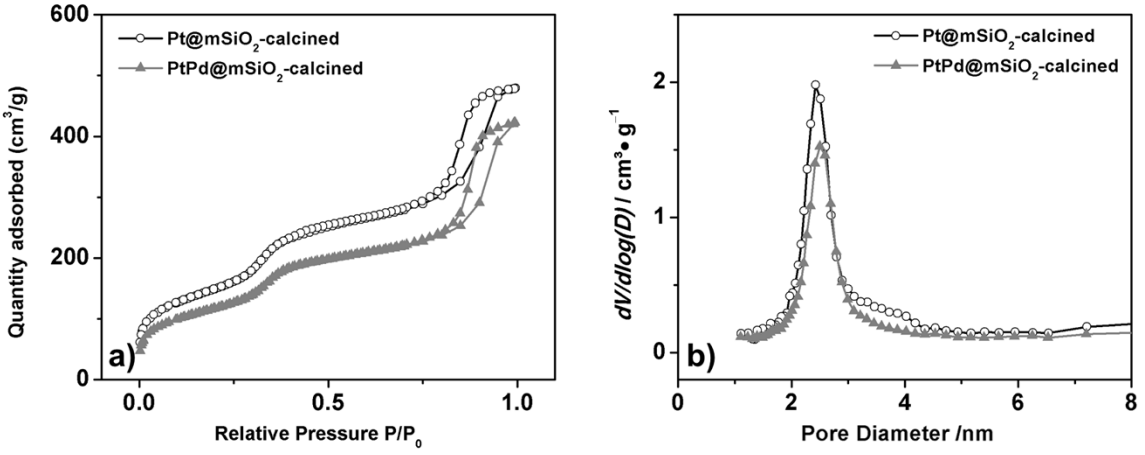

Figure S1. a) Nitrogen adsorption isotherms and b) Pore size distributions of $Pt@mSiO_2$ and $PtPd@mSiO_2$.

Table S1. Summary of BET specific area, average pore size and pore volume of $Pt@mSiO_2$ and $PtPd@mSiO_2$.

Items [a]	Specific area /$cm^2 \cdot g^{-1}$	Pore size /nm [b]	Pore volume /$cm^3 \cdot g^{-1}$
$Pt@mSiO_2$	503.4	2.4	0.66
$PtPd@mSiO_2$	396.0	2.5	0.59

[a] All samples were calcined at 350 ˚C in air for 4 hrs and reduced at 300 ˚C in 5% Ar/H_2 for 2 hrs before BET characterization; [b] Pore sizes were determined from BJH pore size distribution.

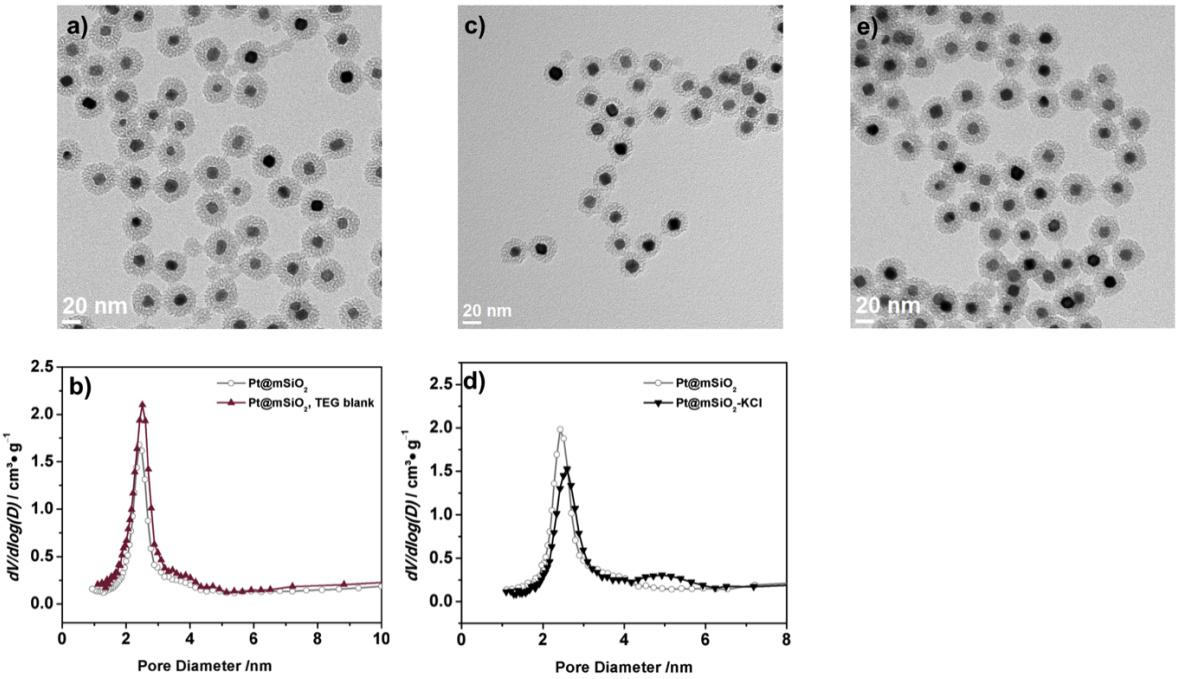

Figure S2. a) TEM image of $Pt@mSiO_2$ blank control in TEG; b) Pore size distributions of $Pt@mSiO_2$ (hollow circles) and $Pt@mSiO_2$–blank control (russet triangles); c) TEM image of $Pt@mSiO_2$ with the addition of 4 equivalents of KCl in TEG using the same heating program employed for the synthesis of $PtPd@mSiO_2$; and d) Pore size distributions of $Pt@mSiO_2$ (hollow circles) and $Pt@mSiO_2$–KCl control (black down triangles); and e) $PtPd@mSiO_2$ after Pd etched by HNO_3 when using fresh $PtPd@mSiO_2$ in solution without drying as the starting material.

Table S2. Summary of Si contents in the supernatant solutions of various samples.

Entry	Sample	Si contents (mg/mL)
1	TEG blank during ICP	0.14 ± 0.04
2	TEG control	0.21 ± 0.01
3	Pt/TEG	0.24 ± 0.02
4	PtPd/TEG	0.29 ± 0.01

The TEG blank (Entry 1, Table S2) corrects the baseline "Si contents" from COH interference as with the same TEG concentration as in our samples. Entry 2-3 in Table S2 are control samples that have been treated under the same synthetic conditions as the PtPd NPs (Entry 4). The Si contents in the three samples were evaluated as shown in the Table S2: for Entry 2, only TEG presents without the addition of either Pt@$mSiO_2$ seeds or K_2PdCl_4 salts; for Entry 3, Pt@$mSiO_2$ seeds presents alone in TEG; and for Entry 4, typical synthetic conditions with Pt@$mSiO_2$ seeds and K_2PdCl_4 salts. The Si content in each Entry was measured and averaged from three samples prepared in three independent experiments.

The entry 2 shows increasing Si content comparing to TEG blank, which suggests that the glass container for synthesis is a source of Si. When only Pt@$mSiO_2$ seeds present (Entry 3, Table S2), the amount of Si contents do not soar up much compared with TEG control (Entry 2). However, the sample in Entry 4 shows an obvious increase of Si when Pd salt was introduced to Pt@$mSiO_2$ seeds, which might indicate that $mSiO_2$ was etched during synthesis. It is notable that TEG interference will strongly shield Si signal and it is uncertain to avoid the $mSiO_2$ residues during the centrifugation process to separate the supernatant. Even though the exact quantities of Si contents may have some uncertainty, the trend of Si content increasing is consistent during the Pd deposition, which supports the $mSiO_2$ etching mechanism.

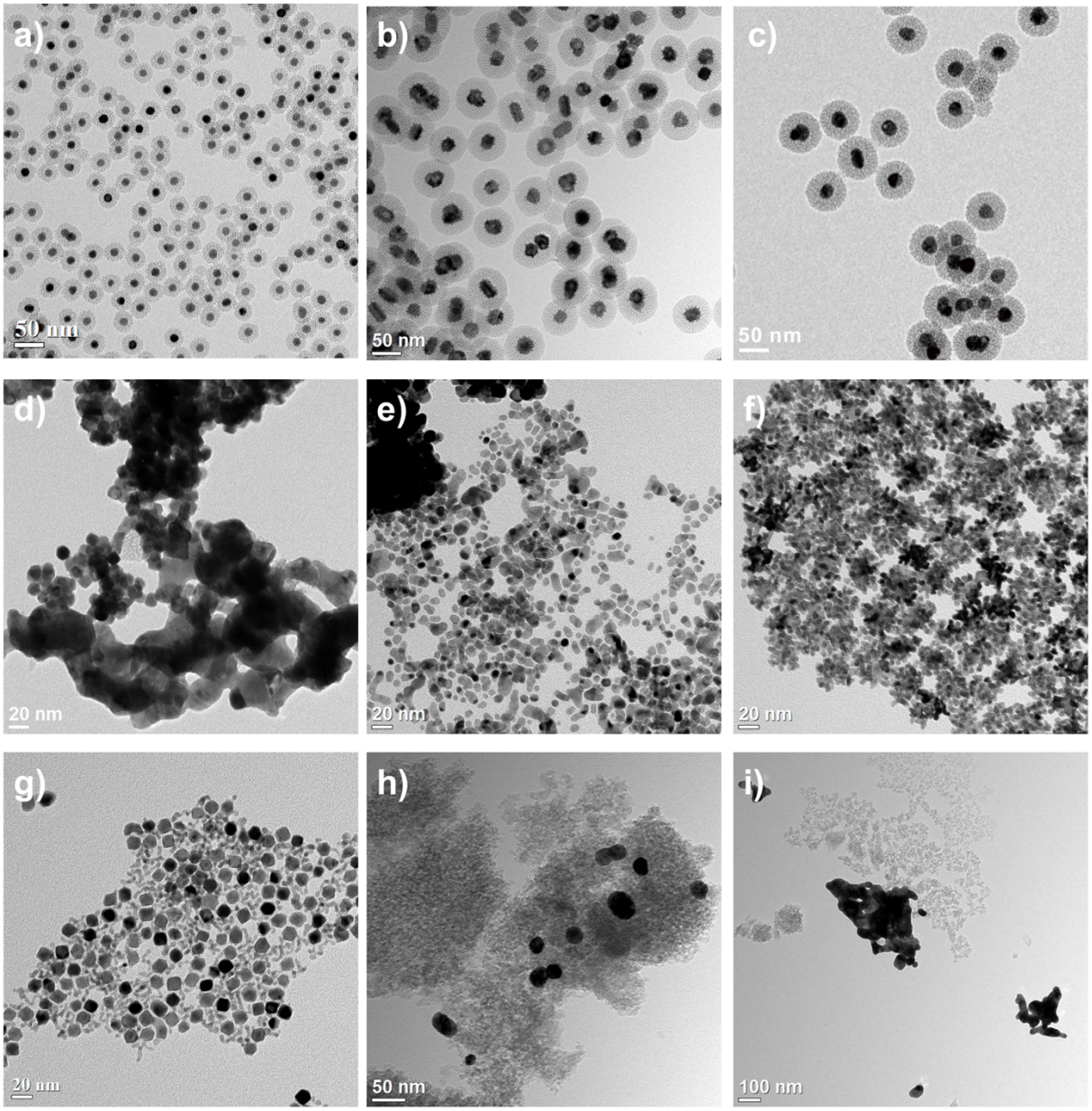

Figure S3. TEM images of a) $PtPd@mSiO_2$ synthesized by reducing $Pt@mSiO_2$ with $Pd(acac)_2$ in TEG; b) $PdPt@mSiO_2$ synthesized by reducing $Pd@mSiO_2$ and H_2PtCl_6 in TEG (slightly isolated NPs observed); c) $PdPt@mSiO_2$ by reducing $Pd@mSiO_2$ and H_2PtCl_6 in oleylamine; d) Pt NPs and K_2PdCl_4 directly reduced in TEG without the addition of organic capping agents and without $mSiO_2$ shell protection; e) Pt NPs, K_2PdCl_4 and additional PVP (80 equivalent molar ratio to Pt) reduced in TEG; f) Flower–like PdPt NPs by reducing Pd NPs and H_2PtCl_6 in oleylamine; g) Pt NPs and $Pd(acac)_2$ reduced in oleylamine; h), i) Flower–like PdPt NPs supported on silica gel after 350 ˚C calcination and 300˚C reduction.

Table S3. ICP-MS results of all PtM@$mSiO_2$ nanostrucrures (M=Pd, Ni, Cu and Rh).

Items	Added Pt/M, molar	Major metal /wt.%	Secondary metal /wt.%	Actual M/Pt, molar
Pt@$mSiO_2$	–	42% Pt	–	–
Pd@$mSiO_2$	–	38% Pd	–	–
$PtPd_{0.50}$@$mSiO_2$	1:0.5 Pt/Pd	28% Pt	7.5% Pd	1:0.50 Pt/Pd
$PtPd_{0.74}$@$mSiO_2$	1:0.7 Pt/Pd	28% Pt	11% Pd	1:0.74 Pt/Pd
$PtPd_{1.1}$@$mSiO_2$	1:1 Pt/Pd	31% Pt	18% Pd	1:1.1 Pt/Pd
$PtPd_{1.6}$@$mSiO_2$	1:1.6 Pt/Pd	30% Pt	27% Pd	1:1.67 Pt/Pd
$PdPt_{0.48}$@$mSiO_2$	0.5:1 Pt/Pd	19% Pt	22% Pd	0.48:1 Pt/Pd
$PdPt_{1.1}$@$mSiO_2$	1:1 Pt/Pd	–	–	1.1: 1 Pt/Pd
PtPd@$mSiO_2$–$Pd(acac)_2$	1:1 Pt/Pd	–	–	1:(0.5 – 0.7) Pt/Pd
PtNi@$mSiO_2$	1:1 Pt/Ni	28% Pt	8.0% Ni	1:0.96 Pt/Ni
PtCu@$mSiO_2$	1:1 Pt/Cu	31% Pt	6.8% Cu	1:0.68 Pt/Cu
PtRh@$mSiO_2$	1:1 Pt/Rh	22% Pt	12% Rh	1:1.1 Pt/Rh

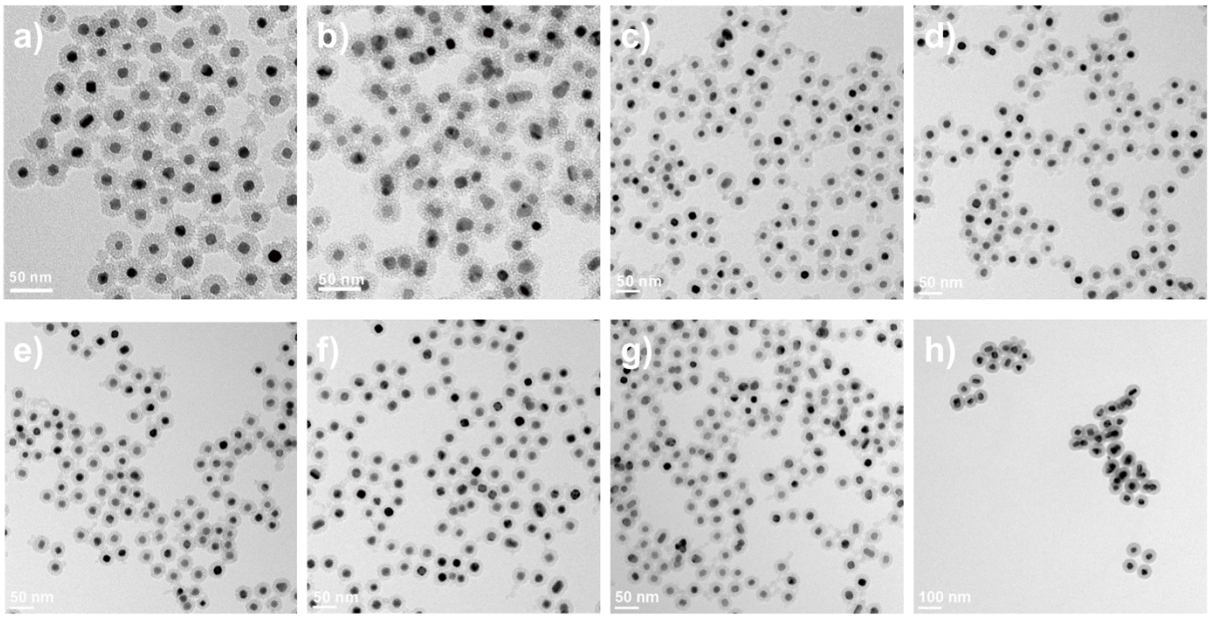

Figure S4. TEM images of a) $Pt@mSiO_2$; b) $Pd@mSiO_2$; c) $PtPd_{0.50}@mSiO_2$; d) $PtPd_{0.74}@mSiO_2$; e) $PtPd_{1.1}@mSiO_2$; f) $PtPd_{1.6}@mSiO_2$; g) $PdPt_{0.48}@SiO_2$; and h) $PdPt_{1.1}@mSiO_2$.

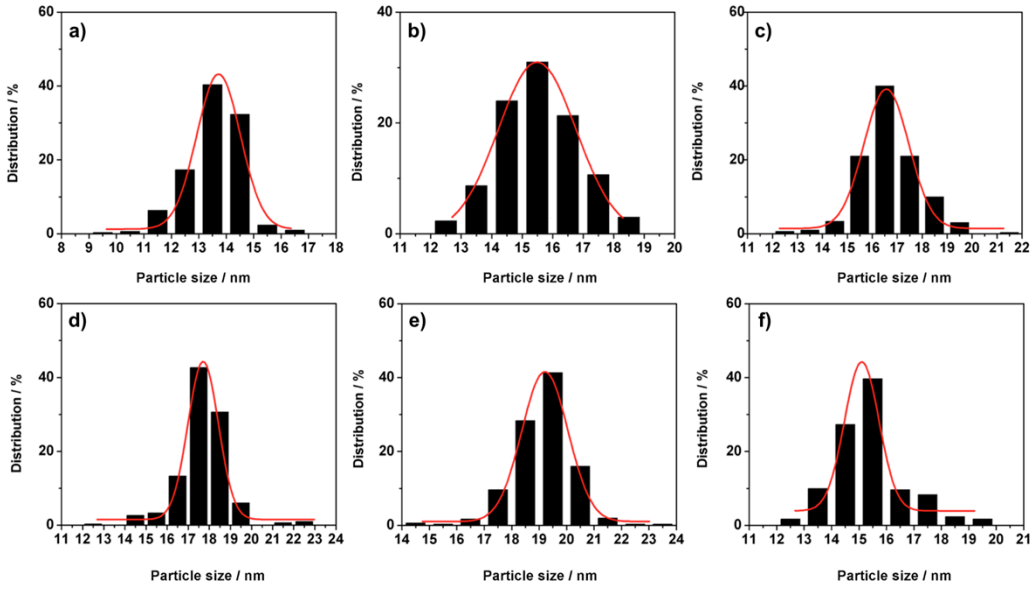

Figure S5. Particle size distributions are acquired by counting 300 particles in TEM images of corresponding samples as shown in Figure S4, a) $Pt@mSiO_2$ (13.6 ± 1.0 nm); b) $PtPd_{0.50}@mSiO_2$ (15.5 ± 1.3 nm); c) $PtPd_{0.74}@mSiO_2$ (16.7 ± 1.2 nm); d) $PtPd_{1.1}@mSiO_2$ (17.7 ± 1.2 nm); e) $PtPd_{1.6}@mSiO_2$ (19.1 ± 1.1 nm); and f) $PdPt_{0.48}@mSiO_2$ (15.4 ± 1.3 nm).

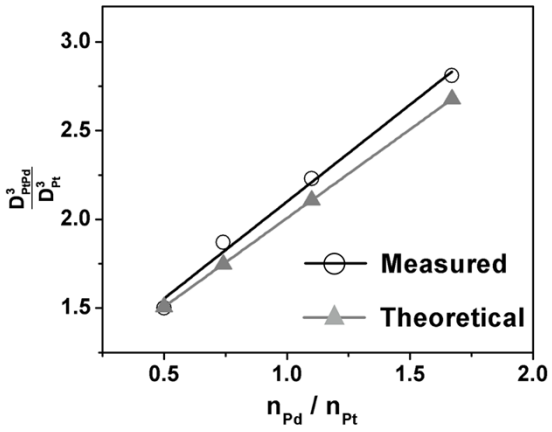

Measured:

$$\frac{D^3_{PtPd}}{D^3_{Pt}} = 1.1\frac{n_{Pd}}{n_{Pt}} + 1.0$$

Theoretical:

$$\frac{D^3_{PtPd}}{D^3_{Pt}} = 1.0\frac{n_{Pd}}{n_{Pt}} + 1.0$$

Equation S1. Mathematical conversion of measured (black circles) and theoretical slopes (grey triangles) in the above figure pertaining to Pd/Pt molar ratios and the volumetric increase of PtPd bimetallic cores.

Calculation details in equation S1:

Assuming both Pt and PtPd core are spherical in shape, the volume increase of PtPd core due to Pd contents depositing on Pt core can be interpreted based on metal core diameters as below, which is also the increase along the y–axis.

$$\frac{V_{PtPd}\text{-}V_{Pt}}{V_{Pt}} = \frac{V_{Pd}}{V_{Pt}} = \frac{D^3_{PtPd}\text{-}D^3_{Pt}}{D^3_{Pt}}$$

And thus, it is possible to find the relationship between volume increase and Pd to Pt ratios in the above figure.

$$\frac{D^3_{PtPd}}{D^3_{Pt}} \propto \frac{n_{Pd}}{n_{Pt}}$$

The fitted linear relationship of measured data (black circles) is described as:

$$\frac{D^3_{PtPd}}{D^3_{Pt}} = 1.1\frac{n_{Pd}}{n_{Pt}} + 1.0$$

The slope of the theoretical line (grey triangles) was calculated based on bulk Pt and Pt metal density as above:

$$\text{Theoretical Slope} = \frac{D^3_{PtPd}\text{-}D^3_{Pt}}{D^3_{Pt}}\frac{n_{Pt}}{n_{Pd}} = \frac{V_{Pd}}{V_{Pt}}\frac{n_{Pt}}{n_{Pd}}$$
$$= \frac{M_w(Pt)}{M_w(Pd)}\frac{d_{Pd}}{d_{Pt}} = \frac{195.1\ g\cdot mol^{-1}}{106.4\ g\cdot mol^{-1}}\frac{12\ g\cdot cm^{-3}}{21.4\ g\cdot cm^{-3}} = 1.0$$

So we can describe the theoretical line above as:

$$\frac{D^3_{PtPd}}{D^3_{Pt}} = 1.0\frac{n_{Pd}}{n_{Pt}} + 1.0$$

The slopes of the theoretical line (1.0) and measure line (1.1) are fairly close, which indicates that Pd contents are introduced into Pt@mSiO_2 seed with high efficiency.

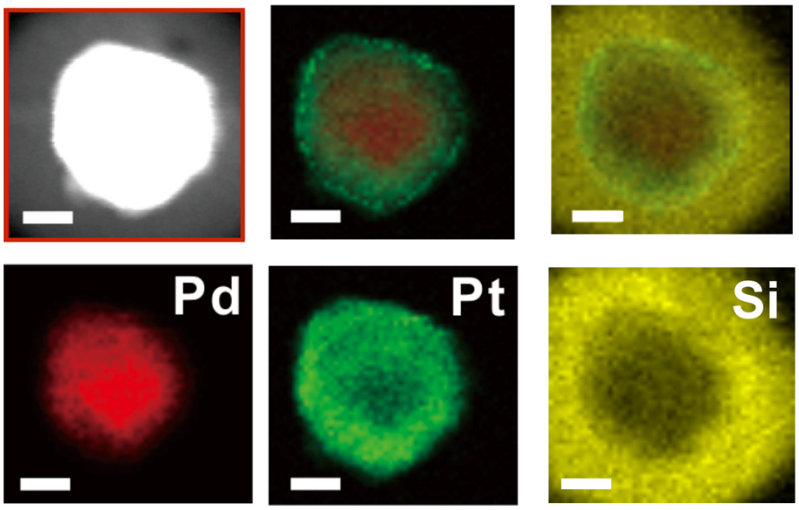

Figure S6. The Pt, Pd and Si elemental mappings of PdPt@mSiO_2. The scale bars are all 10 nm. The PdPt core is almost resident within the mSiO_2 shell.

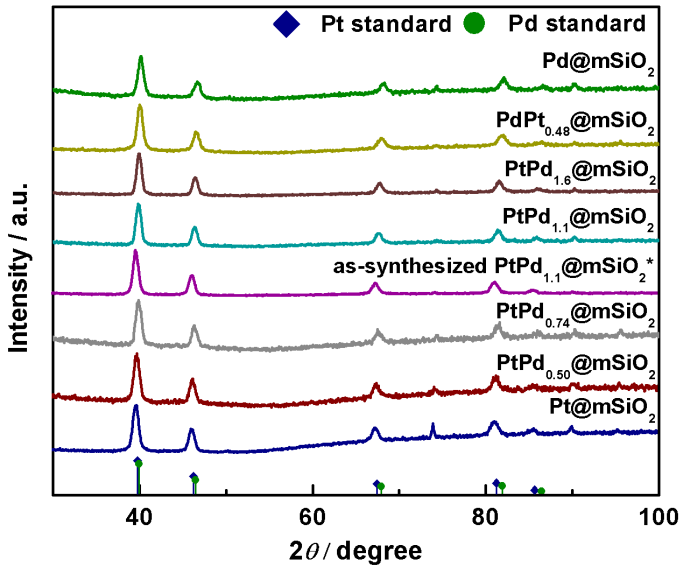

Figure S7. PXRD patterns of PtPd@$mSiO_2$ samples with various Pt/Pd ratios after calcination and reduction.

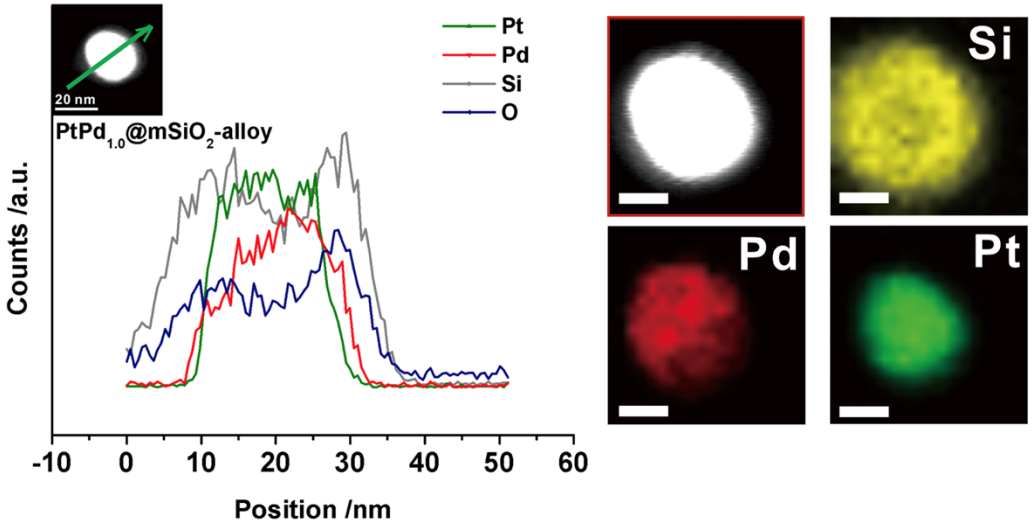

Figure S8. EDS line scans and elemental mappings of alloy PtPd@$mSiO_2$. The scale bars in elemental mappings figure are all 10 nm.

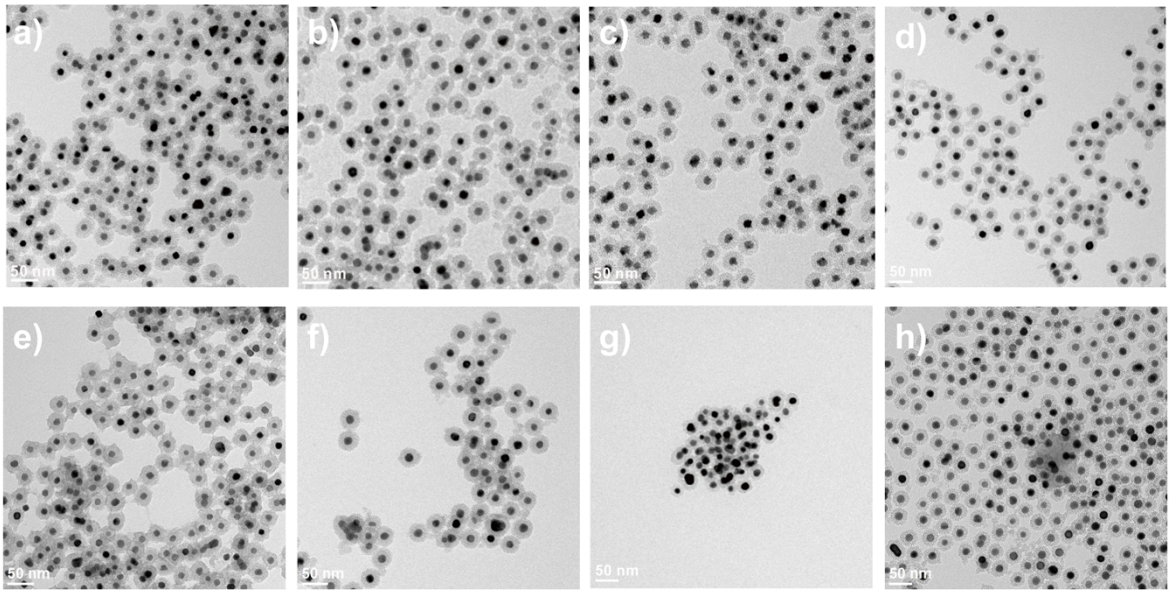

Figure S9. TEM images of as–synthesized PtM@$mSiO_2$: a) PtNi@$mSiO_2$; b) PtCu@$mSiO_2$; c) PtRh@$mSiO_2$; and d) $PtPd_{1.1}$@$mSiO_2$, and PtM@$mSiO_2$ after thermal treatment: e) PtNi@$mSiO_2$ after 350˚C annealing; f) PtCu@$mSiO_2$ after 350 ˚C annealing; g) PtRh@$mSiO_2$ after 500 ˚C annealing; and h) $PtPd_{1.1}$@$mSiO_2$ after 350˚C annealing.

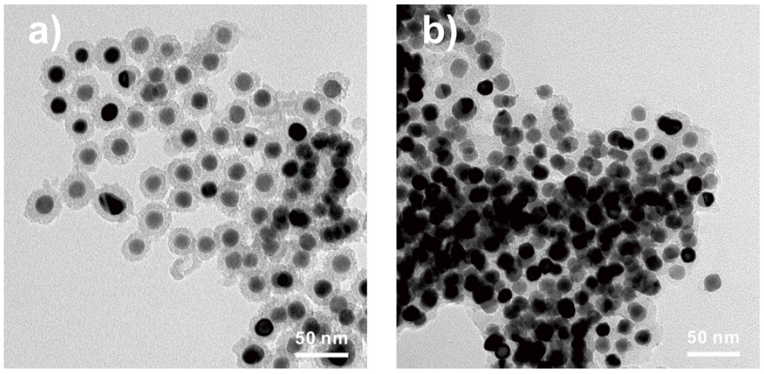

Figure S10. TEM image of a) PtPd@$mSiO_2$ after 350 ˚C calcination, 300 ˚C reduction and collected after reaction; and b) PtPd@$mSiO_2$ after 6 runs before catalyst deactivation.

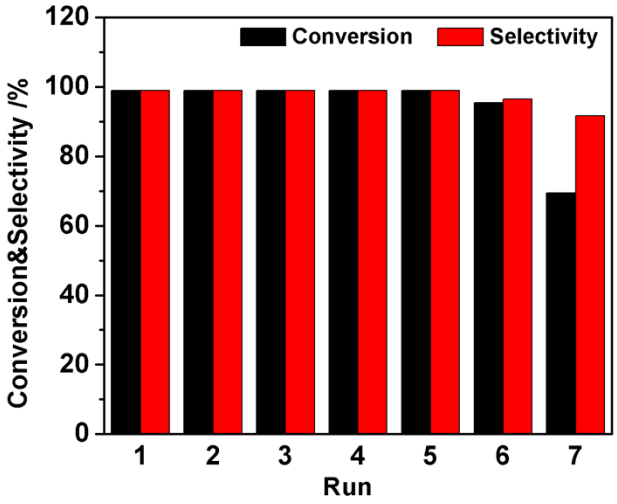

Figure S11. Conversion and selectivity of PtPd@mSiO$_2$ catalyst with 7 runs for nitrobenzene hydrogenation.

Table S4. The resuablity of PtPd@mSiO$_2$ in nitrobenzene hydrogenation. [a)]

Run number	Conversion (%)	Selectivity (%)
1	>99	>99
2	>99	>99
3	>99	>99
4	>99	>99
5	>99	>99
6	95.4	96.5
7	69.5	91.7

[a)] All reaction conditions were controlled the same, and the catalyst was centrifuged down and used directly for the next cycle.

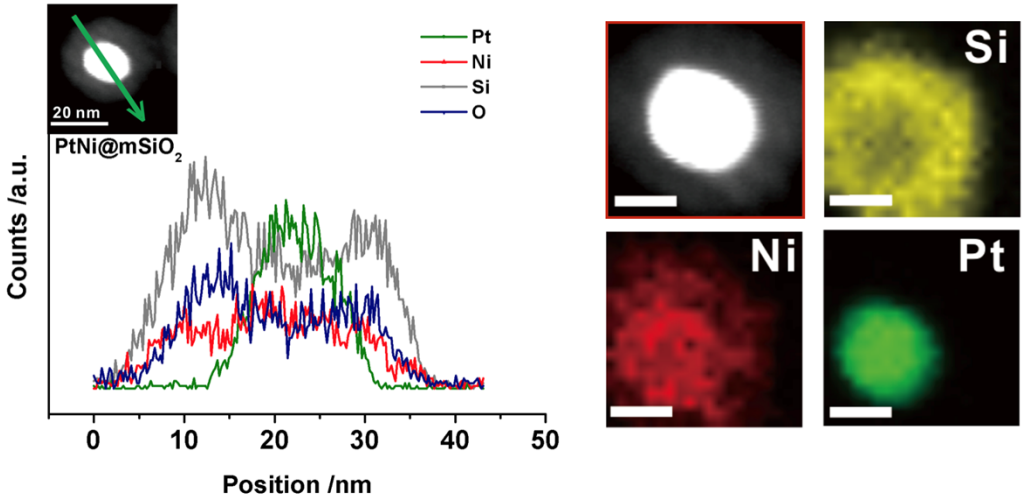

Figure S12. EDS line scans and elemental mappings of $PtNi@mSiO_2$. The scale bars in elemental mappings figure are all 10 nm. Ni is dominant around the area of the original Pt core, however some Ni signals are observed spreading within the $mSiO_2$ framework.

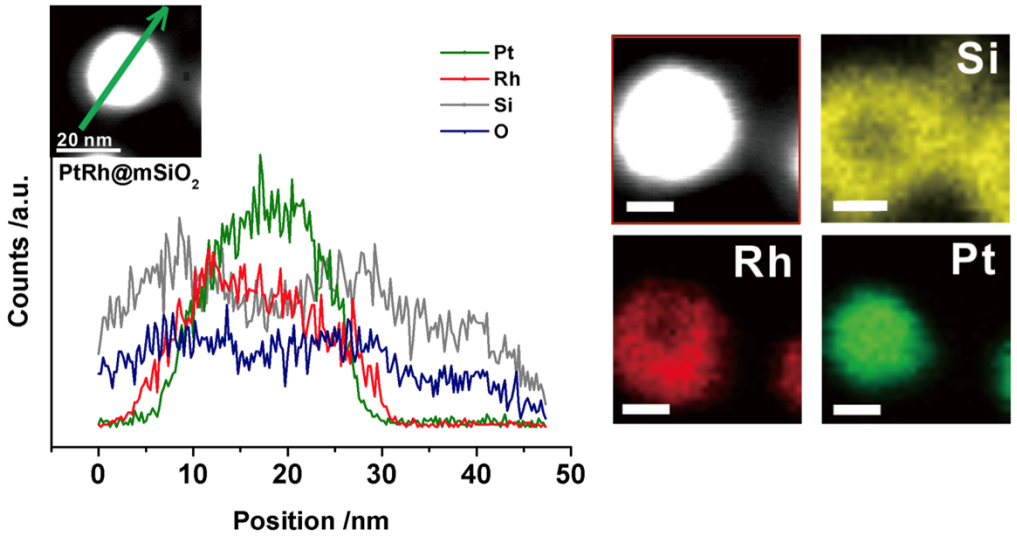

Figure S13. EDS line scans and elemental mappings of $PtRh@mSiO_2$. The scale bars in elemental mappings figure are all 10 nm. Rh is deposited on the Pt core to form the Pt core/Rh shell structure. Rh signals are mixed well with Pt at 10-25 nm region, which indicates that PtRh alloy phase is also present.

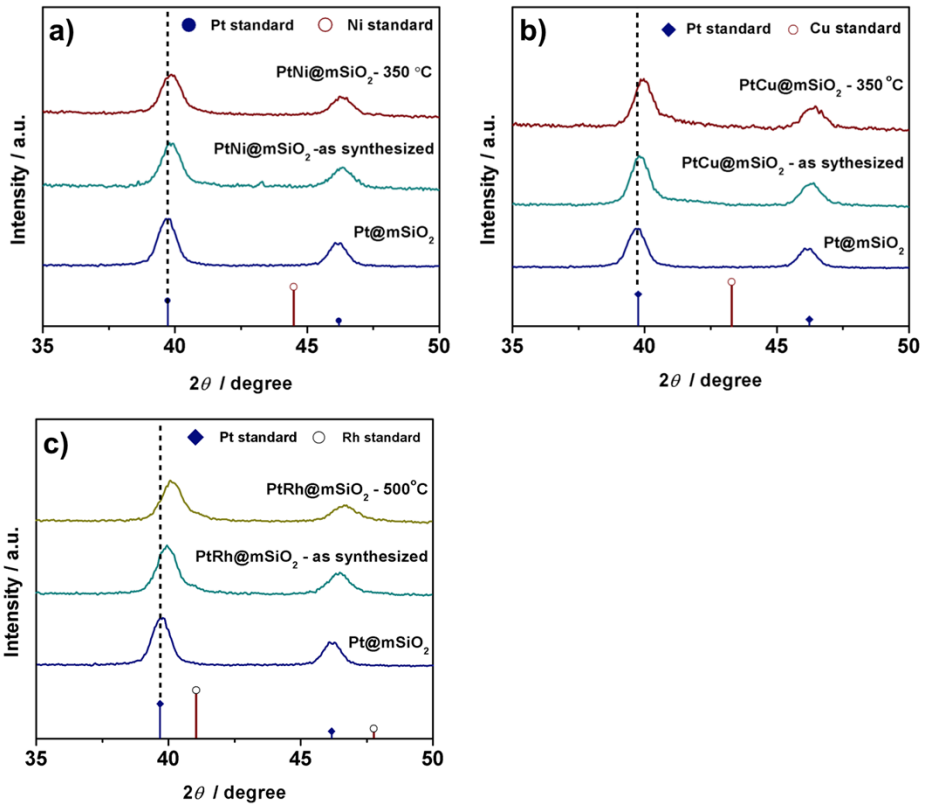

Figure S14. PXRD patterns of as–synthesized and annealed PtM@mSiO$_2$ samples: a) PtNi@mSiO$_2$; b) PtCu@mSiO$_2$; and c) PtRh@mSiO$_2$.

References

1. S. H. Joo, J. Y. Park, C. K. Tsung, Y. Yamada, P. Yang, G. A. Somorjai, *Nat. Mater.* **2009**, *8*, 126–131.

2. N. Ortiz, R. G. Weiner, S. E. Skrabalak, *ACS Nano* **2014**, *8*, 12461–12467.

3. Y. Gao, C. Wang, J. Guan, D. Ma, Xinhe Bao, *Chem. Commun.* **2011**, *47*, 2432–2434.